RMetS
Royal Meteorological Society

Assimilation of GBVTD-retrieved winds from single-Doppler radar for short-term forecasting of super typhoon *Saomai* (0608) at landfall

Kun Zhao,[a,b] Ming Xue[a,b,c*] and Wen-Chau Lee[d†]

[a]*Key Laboratory for Mesoscale Severe Weather/MOE and School of Atmospheric Sciences, Nanjing University, China*
[b]*Center for Analysis and Prediction of Storms, University of Oklahoma, Norman, Oklahoma, USA*
[c]*School of Meteorology, University of Oklahoma, Norman, Oklahoma, USA*
[d]*Earth Observing Laboratory, National Center for Atmospheric Research, Boulder, Colorado, USA*

*Correspondence to: M. Xue, Center for Analysis and Prediction of Storms, University of Oklahoma, 120 David L. Boren Blvd, Norman, OK 73072, USA. E-mail: mxue@ou.edu

†The National Center for Atmospheric Research is sponsored by the National Science Foundation.

A single-Doppler wind retrieval method called the Ground-Based Velocity-Track Display technique (GBVTD) has been developed in recent years to retrieve horizontal circulations of tropical cyclones. The technique is able to retrieve axisymmetric tangential and radial winds, asymmetric tangential winds for wave numbers 1–3, and along-beam mean winds in tropical cyclones. It has been successfully applied to tropical cyclone monitoring and warning. This study explores, for the first time, the assimilation of GBVTD-retrieved winds into a tropical cyclone prediction model, and examines its impact relative to that of directly assimilated radial velocity data. super typhoon *Saomai* (2006), the most intense landfalling typhoon ever recorded in China, is chosen as the test case, and data from the coastal operational radar at Wenzhou, China, are used. The ARPS 3DVAR system is used to assimilate either the radial velocity data directly or the GBVTD-retrieved winds, at 30 min intervals for 2 hours.

The assimilation of the GBVTD-retrieved winds results in much improved structure and intensity analyses of *Saomai* compared to those in the Japan Meteorological Agency mesoscale reanalysis and compared to the analysis assimilating radial velocity (V_r) data directly. The ability of the GBVTD method in providing wind information covering the full circle of the inner-core circulation is the primary reason for its superior performance over direct assimilation of V_r data; for the latter, the azimuthal data coverage is often incomplete. With the improved initial conditions, the subsequent forecasts of typhoon intensity, track and precipitation are also improved. The improvements to both track and intensity predictions persist over a 12-hour forecast period, which is mostly after landfall. Subjective and quantitative evaluations of the precipitation and circulation patterns show consistent results. A further sensitivity experiment shows that the axisymmetric wind component in the GBVTD retrieval has the dominant impact on the prediction. Copyright © 2011 Royal Meteorological Society

Key Words: GBVTD retrieval; radar data assimilation; typhoon prediction

Received 12 July 2010; Revised 6 September 2011; Accepted 17 October 2011; Published online in Wiley Online Library 24 November 2011

Citation: Zhao K, Xue M, Lee W-C. 2012. Assimilation of GBVTD-retrieved winds from single-Doppler radar for short-term forecasting of super typhoon *Saomai* (0608) at landfall. *Q. J. R. Meteorol. Soc.* **138**: 1055–1071. DOI:10.1002/qj.975

1. Introduction

The landfalling tropical cyclone (TC) is one of the most deadly and costly natural hazards; accurate prediction of their track and intensity are crucial for the protection of life and property. Over the past several decades, TC track forecasting has improved steadily due to the increased use of satellite and other observations over the ocean and improved numerical weather prediction (NWP) models. As noted in Elsberry (2005), prediction of the TC track has advanced to the point where the original goals of the US Weather Research Program have been achieved. However, TC intensity and structure forecasting has improved very slowly (Houze *et al.*, 2007; Davis *et al.*, 2008). One of the main reasons for this slow improvement is the lack of accurate initial conditions that capture the internal structures, including precipitation bands and eyewall, in TCs (Davis *et al.*, 2008).

The Doppler weather radar is the only instrument that can observe the three-dimensional structure of TCs with high spatial and temporal resolutions. For landfalling TCs, coastal Doppler radars often can provide such data coverage near their landfall. A Doppler radar, however, only observes the along-beam component of the 3D wind field. Although dual-Doppler analyses can provide a relatively accurate estimation of the full winds, regions with dual-Doppler coverage are usually rather limited in spatial coverage. As a result, assimilating single-Doppler radar data in NWP models remains a primary option where effective assimilation and/or retrieval techniques are necessary. Several recent studies assimilated coastal Doppler radial velocity (V_r) data from multiple radars, using three-dimensional variational (3DVAR) methods (Zhao *et al.*, 2006; Xiao *et al.*, 2007; Zhao and Jin, 2008; Zhao *et al.*, 2008; Zhao and Xue, 2009) or ensemble Kalman filter (EnKF) (Zhang *et al.*, 2009; Dong and Xue, 2010). While the results are encouraging, assimilating radar data remains a challenging problem and its application to hurricane prediction is a rather new area of research. With 3DVAR-based methods, the cross-beam components of winds are often not retrieved very well in the absence of dual- or multi-Doppler coverage and the restriction of data to precipitation regions often leads to patchy analysis increments that lack spatial continuity as well as balance among state variables. The EnKF method is theoretically more advanced but its practical application on operational TC forecasts still requires more research.

Traditionally, the initialization of TCs in NWP models often relies on the use of a so-called bogus vortex that typically includes an axisymmetric component constructed based on few estimated parameters on TC size and intensity and an asymmetric component extracted from the background fields (Kurihara *et al.*, 1993; Zou and Xiao, 2000; Xiao *et al.*, 2009). While proven helpful, the idealization involved in the construction of such vortices has its own problems. The best solution should be to analyse/construct the TC vortex, including its 3D structures, using direct observations as much as possible.

In recent years, a single-Doppler wind retrieval method, called the Ground-Based Velocity-Track Display technique (GBVTD) (Lee *et al.*, 1999, LJCD hereafter), has been developed to retrieve two-dimensional primary circulations of landfalling TCs at different altitudes. GBVTD has been successfully applied to several landfalling TC cases (Lee *et al.*, 2000; Harasti *et al.*, 2004; Lee and Bell, 2007; Zhao *et al.*, 2008) for potential monitoring and warning applications. It has been shown that GBVTD is capable of retrieving horizontal winds of mature TCs with an accuracy of about 2 m s^{-1} (Harasti *et al.*, 2004). Lee *et al.* (2006) derived the divergence and vertical velocities using vorticity equation and high-temporal-resolution GBVTD-retrieved winds in Hurricane Danny (1997). In a sense, GBVTD can be considered a more sophisticated vortex-fitting technique that can provide more accurate 3D structures than does a typical bogus vortex. Assimilating GBVTD-retrieved winds into NWP models for TC forecasting can potentially outperform commonly used bogus vortex techniques, or even direct assimilation of radial velocity data. This has, however, never been attempted so far, and is the focus of this study.

To build up dynamically consistent TCs from radar observations, an assimilation method that takes advantage of the high temporal and spatial resolutions of the data is necessary. A procedure combining the 3DVAR and complex cloud analysis scheme from the Advanced Regional Prediction System (ARPS; Xue *et al.*, 2003) has proven to be effective in initializing mid-latitude thunderstorms in a number of studies (e.g. Hu *et al.*, 2006, H06 hereafter). Recently, it has been successfully applied to the analysis and retrospective forecasting of the landfalling Hurricane Ike (2008) in the Gulf of Mexico region of the USA (Zhao and Xue, 2009). The ARPS 3DVAR (Gao *et al.*, 2004) can analyse either radar radial velocity or radar-retrieved wind data, while the cloud analysis procedure determines the cloud and hydrometeor fields from reflectivity (Z) and other cloud observations and adjusts in-cloud moisture and temperature (Brewster, 2002; H06).

Encouraged by the above results, this study explores for the first time the assimilation of GBVTD-retrieved winds (V_{GBVTD}) within the ARPS 3DVAR framework for the analysis and prediction of super typhoon *Saomai* (2006), the strongest landfalling typhoon ever recorded in China. During *Saomai*'s landfall, its inner core region was fully observed by China Next Generation Radar 1998 Weather Surveillance Doppler (CINRAD WSR-98D) radar located at Wenzhou (WZRD), Zhejiang Province, from 0000 to 1200 UTC, 10 August 2006, at 6-minute volume scan intervals. The axisymmetric kinematic and dynamic structures of its inner core region were recently examined using GBVTD-retrieved winds from WZRD (Zhao *et al.*, 2008). In this study, the V_{GBVTD} data are assimilated through 30-minute intermittent assimilation cycles during a 2-hour period before landfall. The impacts of assimilating V_{GBVTD} on the intensity, rainband structure, track and quantitative precipitation prediction of *Saomai* will be examined, and compared with direct assimilation of radial velocity data, V_r.

This paper is organized as follows. Section 2 describes the assimilation method, domain configuration, model setup and processing of observations. The analysis results are presented and discussed in section 3, while the prediction results are in section 4. Summary and conclusions are presented in section 5.

2. Radar data, wind retrieval, and data assimilation

2.1. Radar data processing and quality control

In this paper, full-resolution level II data from WZRD are used as the initial input. The WZRD operated in the

volume coverage pattern 21 (VCP21) scanning mode of the US WSR-88D standard, which consists of nine elevations starting at 0.5° and ending at 19.5° with a maximum Doppler range of 150 km. With large volumes of radar observations that are recorded at a higher resolution than the forecast model grid spacing (3 km horizontal in this study), data thinning and careful quality control of the observations become necessary. For quality control, we first use the quality control procedures within the 88d2arps program available in the ARPS system (Brewster *et al.*, 2005) to remove/correct erroneous observations, including velocity de-aliasing and ground clutter removal. As described in Brewster *et al.* (2005), the velocity unfolding utilizes a horizontal mean profile derived from an analysis background to estimate the gate-to-gate shear due to mean vertical shear, and check the deviations in the data from this shear for folding problems. Several additional steps are involved in performing the velocity unfolding. After the automatic quality control is performed, the data are further examined and edited manually when necessary using the interactive 'SOLO' software (Oye *et al.*, 1995) from NCAR. The final V_r data are then remapped to the model grid points using a local least-square fitting method for use by the 3DVAR analysis; for the GBVTD wind retrieval they are interpolated onto constant-altitude plan position indicators (CAPPIs) in Cartesian coordinates instead.

2.2. GBVTD wind retrieval

The GBVTD technique (LJCD) represents a modification to a fixed-coordinate-system velocity track display (VTD) technique originally proposed by Lee *et al.* (1994); the latter tries to deduce properties of the primary circulations of tropical cyclones from airborne Doppler radar data. Formulated upon a cylindrical coordinate system centred at the TC circulation centre, the GBVTD analysis uses the Doppler velocities along a constant radius to deduce the tangential and radial winds of a vortex via Fourier decomposition, in a way similar to the velocity azimuth display (VAD) technique (Browning and Wexler, 1968). In this study, the V_{GBVTD} data are very similar to those produced in Zhao *et al.* (2008). The domain of the GBVTD analyses extends from the centre of the typhoon to an 80 km radius and from 1 to 10 km in the vertical. Grid spacing is 1 km in the radial and vertical directions, and 4° in the azimuthal direction. Missing data below 2 km height are extrapolated from above using the same method as Lee *et al.* (2006). It is worth pointing out that the extrapolation may not capture the realistic variation of the boundary layer wind profile, thus affecting the low-level wind analysis (investigating alternative profiles is beyond the scope of this study but it is an important issue). Quantities, including the component of mean wind in the direction from the radar to typhoon centre, $V_{\mathrm{M||}}$, the axisymmetric tangential wind, V_{T0}, the axisymmetric radial wind, V_{R0}, and the asymmetric tangential winds for different wave numbers, $V_{\mathrm{T}n}$ ($n = 1, 2, 3$) are deduced by the GBVTD analysis. As pointed out by LJCD, the maximum wave number resolved at each radius varies with the maximum angular data gap; for data having gaps of 30°, 60°, 120°, and 180°, the maximum wave numbers resolved are 3, 2, 1, and 0, respectively. In addition, the unresolved asymmetric radial wind is aliased into the asymmetric tangential winds (LJCD). The unresolved mean wind component perpendicular to $V_{\mathrm{M||}}$, $V_{\mathrm{M}\perp}$, is approximated by the storm motion vector in the direction of $V_{\mathrm{M}\perp}$ (Harasti *et al.*, 2004) and is used to correct V_{T0}. The total GBVTD winds, V_{GBVTD}, contain all components, $V_{\mathrm{M||}}$, $V_{\mathrm{M}\perp}$, V_{T0}, V_{R0}, and $V_{\mathrm{T}n}$ ($n = 1$, 2, and 3), unless stated otherwise.

2.3. The ARPS and ARPS 3DVAR

The non-hydrostatic ARPS prediction model with full physics is used during the assimilation cycles and for the follow-on forecast. The physics options used include the Lin ice microphysics, Goddard long- and short-wave radiation, a two-layer soil model and the turbulent kinetic energy (TKE)-based subgrid-scale turbulence and PBL parametrization (see Xue *et al.*, 2001, for details). A $611 \times 611 \times 53$ grid at 3 km horizontal grid spacing is used (Figure 1). The domain depth is 25 km and the near-surface vertical grid spacing is about 50 m. Initial analysis and lateral boundary conditions (LBCs) for the ARPS model are from the Japan Meteorological Agency (JMA) 6-hourly gridded regional analyses at 20 km horizontal resolution with 20 pressure levels. The JMA analyses were produced using a multivariate 3D optimum interpolation (OI) method to combine first-guess fields from JMA's regional spectral model (RSM) with observations from a variety of platforms (Segami *et al.*, 1989; Onogi, 1998; Tsuyuki and Fujita, 2002).

The ARPS 3DVAR uses an incremental form of the cost function that includes the background, observation, and mass-continuity equation constraint terms. The analysis variables include the three wind components, potential temperature, pressure, and water vapour mixing ratio (Gao *et al.*, 2004). In the current system, the cross-correlations between variables are not included in the

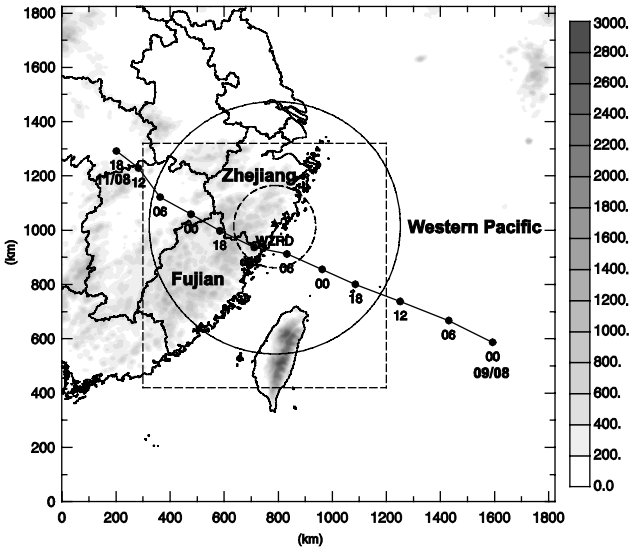

Figure 1. The analysis and prediction domain at 3 km horizontal resolution, with the best track locations of super typhoon *Saomai* marked at 6-hourly intervals from 0000 UTC 9 to 1800 UTC 11 August 2006. The locations of radar stations are shown by the black filled triangles and the ranges of the radar data coverage at WZRD are indicated by dashed circles for radial velocity and solid for reflectivity. The dashed rectangular box indicates the region of reflectivity/rainfall distribution in Figure 13 and the reflectivity/rainfall verification. The grey shading shows the terrain height (m). Also shown are the province borders. *Saomai* made landfall near the border between Zhejiang Province to the north and Fujian Province to the south.

Table I. Description of the radar data assimilation experiments.

Experiment	Assimilation description
CNTL	No radar data assimilation, starting from JMA reanalysis at 0600 UTC 10 August
CNTL00	No radar data assimilation, starting from JMA reanalysis at 0000 UTC 10 August
ExpGV	Assimilating GBVTD-retrieved winds, V_{GBVTD} (defined in section 2)
ExpVr	Assimilating radial velocity data directly
ExpGVNoAsy	Same as ExpGV but without V_{Tn}, $n = 1$, 2 and 3 component

background error covariance. The spatial covariance of background error is assumed spatially homogeneous and Gaussian, and is modelled using a recursive filter. The observation errors are assumed to be uncorrelated so that the observation error covariance matrix is diagonal, and its diagonal elements are specified according to the estimated observation errors. The standard derivations of the observational errors are prescribed to be 1.5 m s^{-1} and 3 m s^{-1} for V_r and V_{GBVTD} data, respectively. In this paper, since V_r data have been edited carefully in objective and subjective quality control steps, the observational errors in V_r are mainly due to inhomogeneities of velocity and reflectivity within a sampling volume, and to representative errors. The error standard deviations of the former generally have a lower bound of about 1 m s^{-1} (Doviak *et al.*, 1976). Our statistics in section 3.1 show that the GBVTD-derived winds have additional 1–2 m s^{-1} differences from observed V_r data in the V_r coverage regions, and hence their errors are expected to be larger. When analysing the radar data, a 10 km horizontal de-correlation scale and a 4 grid-interval vertical de-correlation scale are assumed for the background error covariance in the 3DVAR.

2.4. *Experimental design*

All forecasts use their final analysis at 0600 UTC 10 August 2006 as the initial condition and run for 12 hours, which cover the landfall and post-landfall periods of *Saomai*. The baseline control forecast without radar data assimilation (CNTL) starts the forecast from the 0600 UTC 10 August JMA reanalysis. For comparison purpose, we also include an alternative 'control' forecast (CNTL00) that is the same as CNTL but starts from 0000 UTC JMA reanalysis; this forecast benefits from a 6-hour long spin-up on the high-resolution grid but does not have the benefit of any additional observations up to 0600 UTC. Experiments ExpGV and ExpVr, which assimilate the V_{GBVTD} and Vr data, respectively (see Table I), are designed to examine the impacts of assimilating V_{GBVTD} *versus* V_r data. The data assimilation goes from 0400 to 0600 UTC at 30-minute intervals. Before 0400 UTC, there is a 4-hour pre-forecast period starting from the 0000 UTC JMA reanalysis. To further evaluate the relative importance of the asymmetric component in the GBVTD retrieval, one additional experiment, called ExpGVNoAsy, is performed in which the asymmetric component is excluded.

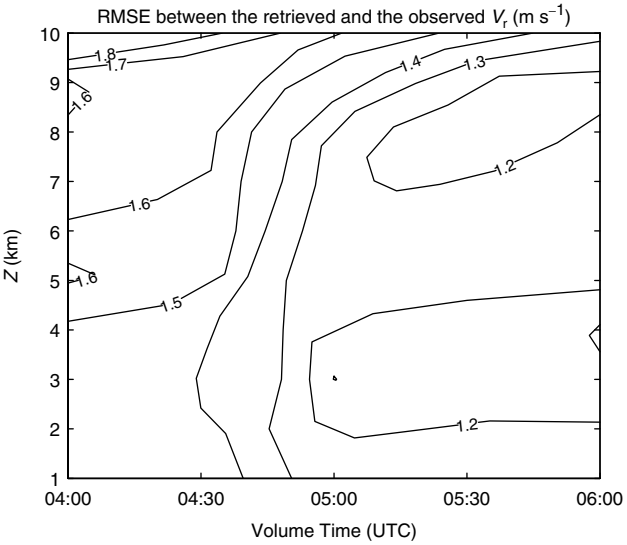

Figure 2. Time–height plot of the root mean square errors between GBVTD-retrieved radial velocity and the observations from WZRD between 0400 UTC to 0600 UTC.

3. Results of GBVTD retrieval and data assimilation

3.1. *Performance of GBVTD retrieval*

To assess the quality of the retrieved velocity, V_{GBVTD}, the root mean square error (RMSE) between the V_r resampled from V_{GBVTD} and the V_r observed by WZRD radar is calculated at various heights from 0400 and 0600 UTC (Figure 2). It is found that the V_r resampled from V_{GBVTD} are consistent and in good agreement with the observed V_r during the analysis period, with RMSEs between 1 and 2 m s^{-1} – well below the observation error of 3 m s^{-1} assumed in ARPS3DVAR analysis. The maximum RMSE of ~1.8 m s^{-1} is found at 0400 UTC, when the centre of *Saomai* just entered the Doppler range of WZRD. The RMSEs decrease to about 1.2 m s^{-1} around 0600 UTC as more circulation of *Saomai* is observed by WZRD.

The retrieved V_{GBVTD} field together with the observed reflectivity Z, the observed V_r, and the resampled V_r from V_{GBVTD} at 3 km height at 0400 (the first analysis time) and 0600 UTC (the final analysis time) are shown in Figure 3. At 0400 UTC, the centre of *Saomai* just entered the coverage of WZRD when the eyewall is located at radius $R = 20$ km, with an organized outer rainband at $R = 60$ km (Figure 3(a)). The WZRD V_r field shows a clear dipole velocity signature associated with the eyewall, but the far side of the eyewall is outside the Doppler range (Figure 3(c)). In comparison to the observed V_r, V_{GBVTD} not only recovers the cross-beam typhoon circulation, but also fills the regions where V_r data are missing (Figure 3(a)). It thereby provides an estimate of the full vortex circulation within an 80 km radius of the typhoon centre. In addition, the V_{GBVTD} field reveals a distinct asymmetric wave number 1 structure with high wind speeds located northeast of the typhoon centre, collocated with the high-reflectivity regions associated with both the eyewall and an outer rainband. The pattern of V_r resampled from V_{GBVTD} is close to the observed V_r, with an RMSE of about 1.4 m s^{-1} (Figure 3(e)), indicating that the observed radial wind information has been retained rather accurately in V_{GBVTD}.

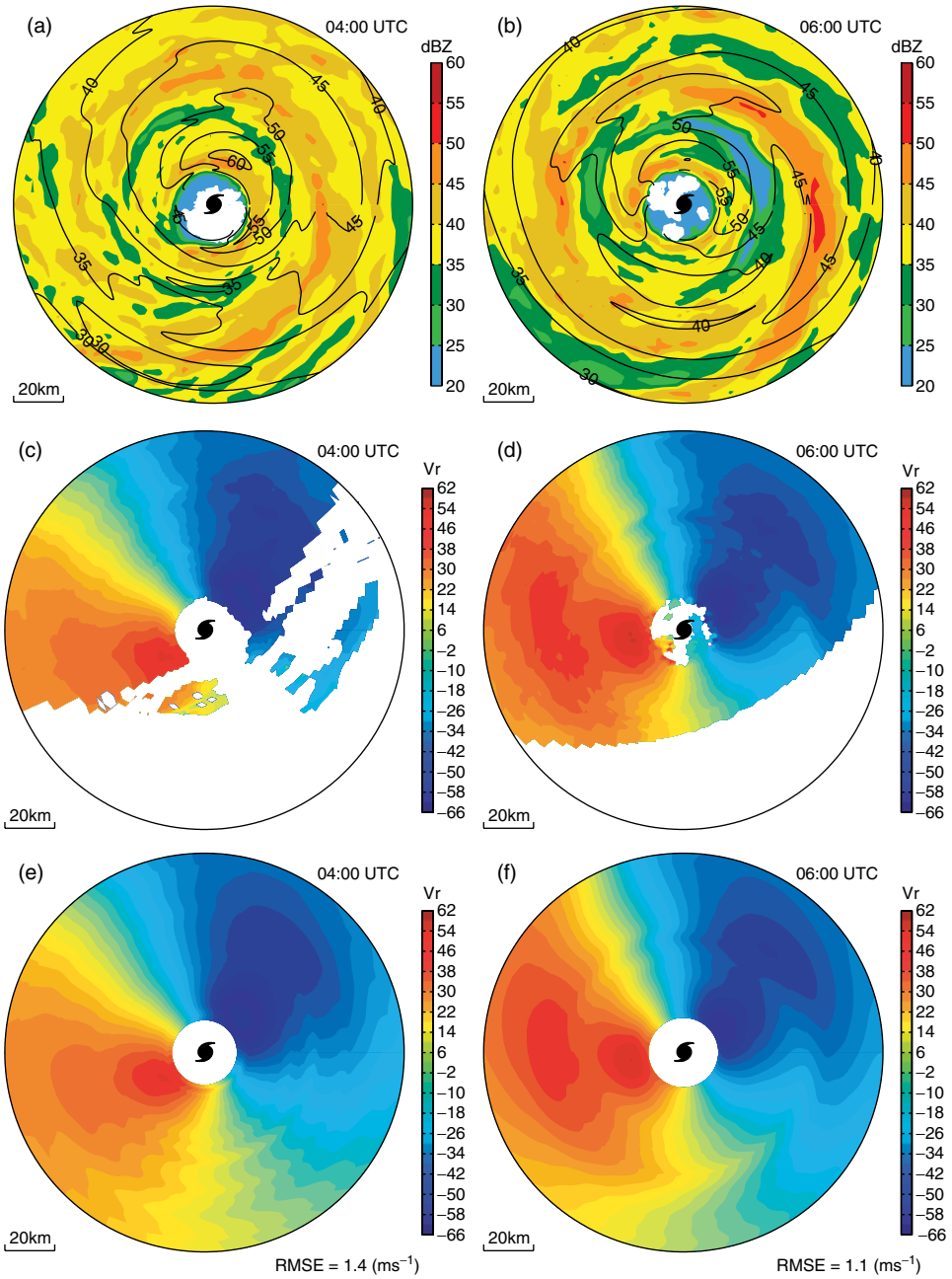

Figure 3. The GBVTD analysis at 3 km height at 0400 (left column) and 0600 UTC (right column). From top to bottom are the GBVTD-retrieved winds (contours, m s^{-1}) overlaid with observed reflectivity (upper panels), the observed Doppler radial velocity from WZRD (middle panels), and radial velocity calculated from the GBVTD-retrieved winds (lower panels). Reflectivity is in colour shades. The RMSE value of the retrieved radial velocity calculated against the observations is shown in the right corner in (e) and (f).

By 0600 UTC, *Saomai* has formed a concentric eyewall structure as its outer rainband evolves into the outer eyewall (Figure 3(b)). Two dipoles, corresponding to maximum and minimum radial velocity pairs at roughly 20 and 55 km radii, respectively, are seen in the WZRD V_r field, corresponding to the inner and outer eyewalls, respectively (Figure 3(d)). The V_{GBVTD} data describe the concentric eyewall feature and the complete inner-core vortex circulation better than the WZRD V_r observations (Figure 3(b, d, f)). The localized wind maximum structures close to the high reflectivity within the outer rainband (southeast of the centre) (Figure 3b) appear to be real; the study of Samsury and Zipser (1995) using *in situ* observations shows that wind maxima are often found within 20 km of reflectivity maxima within TCs.

3.2. *Assimilation of GBVTD-retrieved winds versus V_r data*

Figure 4 shows the horizontal winds of *Saomai* at $Z = 3$ km from the 4-hour forecast starting from the JMA reanalysis at 0000 UTC (Figure 4(a)), which is the background of the first 3DVAR analysis for all assimilation experiments. The figure also shows the results of first analysis from experiments ExpVr (Figure 4(b)) and ExpGV (Figure 4(c)). The typhoon in the background forecast shows a broad eye with an eyewall radius of about 100 km. After V_r or V_{GBVTD} data are assimilated once at 0400 UTC, in ExpVr and ExpGV respectively, the eyewall radius is reduced to ∼30 km and ∼20 km respectively, and the vortex circulation in the inner core region is strengthened with a clear wave number 1 asymmetry pattern (Figure 4(b, c) *versus* (a)). The high

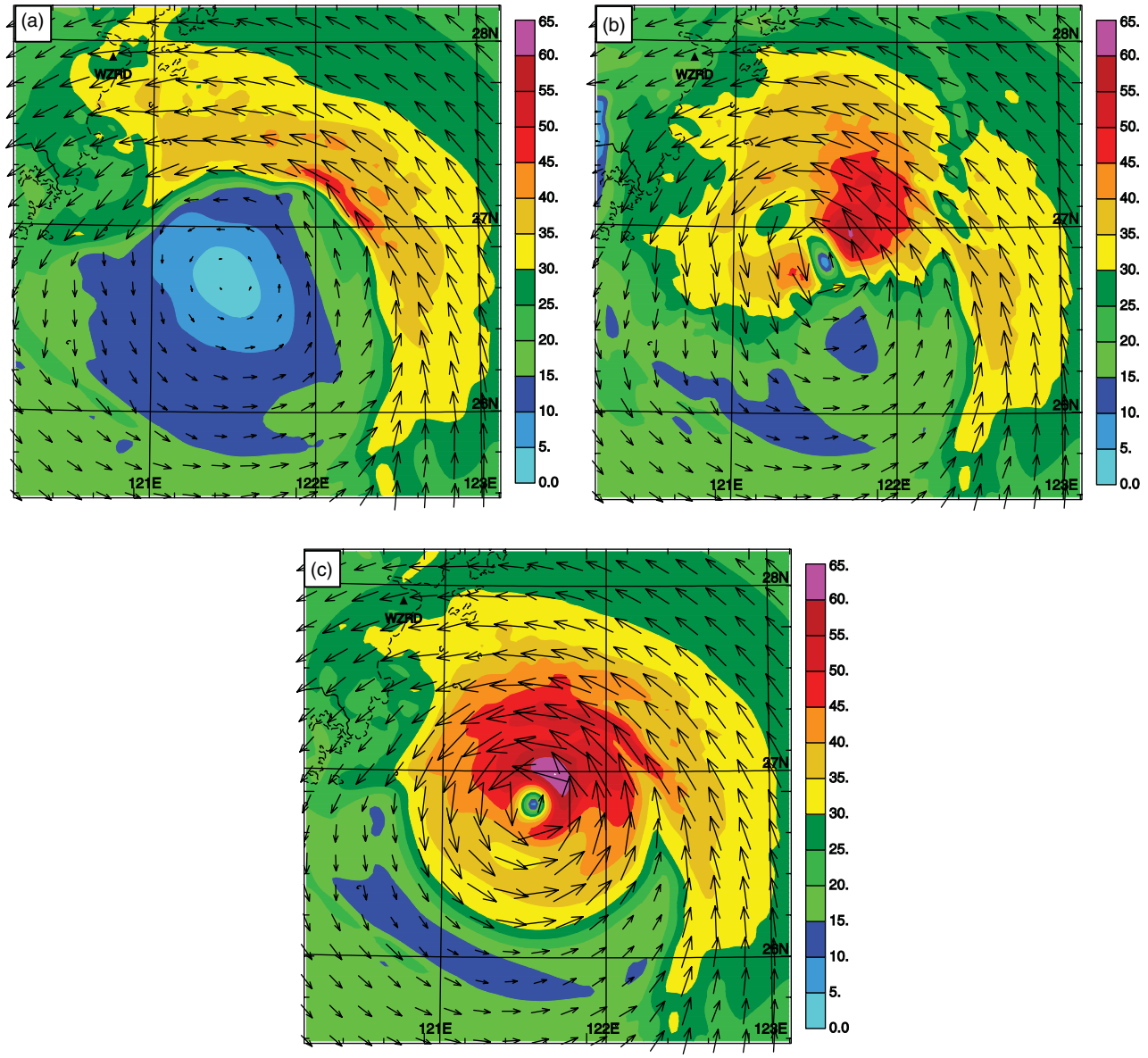

Figure 4. Horizontal wind vectors and speed (color contours, m s^{-1}) at 3 km MSL, at 0400 UTC, the beginning time of the data assimilation window for (a) background forecast starting from JMA reanalysis at 0000 UTC, (b) analysis from ExpVr using radial velocity data, and (c) analysis from ExpGV using GBVTD-retrieved winds.

wind speed is located at the northeast quadrant of the vortex, with the maximum increasing to about 65 m s^{-1} in ExpGV (Figure 4(c)) and 60 m s^{-1} in ExpVr (Figure 4(b)), compared to about 48 m s^{-1} in the background forecast (Figure 4(a)). It is clear that assimilating either V_r or V_{GBVTD} significantly improves the structural details as well as the intensity of the typhoon.

It is interesting to note that major structural differences exist already between the analyses of ExpVr (Figure 4(b)) and ExpGV (Figure 4(c)), after only one analysis at 0400 UTC. First, the shape of the eyewall is elliptical in ExpVr, compared to the more circular shape in ExpGV. The major axis of the ellipse in ExpVr is along the direction connecting the radar and typhoon centre. The horizontal winds in ExpVr are obviously weaker than those in ExpGV at the northwest and southeast quadrants of the typhoon along the major axis of the ellipse. In ExpVr, it is evident that the total wind field (Figure 4(b)) is very close to the observed V_r field, in magnitude and structure (Figure 3(c)), showing that the cross-beam wind component is mostly missing in the 3DVAR analysis from single-Doppler V_r data in this case. A similar situation was reported in Li *et al.* (2010). In contrast, assimilating V_{GBVTD} data produces a more realistic analysis.

Figure 5 shows the sea-level pressure (SLP) and surface wind speed from CNTL (JMA analysis), CNTL00, ExpVr and ExpGV at the end of the data assimilation window (0600 UTC). Clearly, the typhoon intensity in the JMA analysis is too weak (Figure 5(a)); its minimum SLP (MSLP) is about 990 hPa *versus* 920 hPa in the best track data. In this study, the best track data are provided by the Chinese Meteorological Administration (Yu *et al.*, 2007; Song *et al.*, 2010). The best track maximum surface wind (MSW) is about 61 m s^{-1}, while that in CNTL is only about 29 m s^{-1}. CNTL00 (Figure 5(b)) shows a similarly weak vortex to CNTL, with MSLP (MSW) being 984 hPa (36 m s^{-1}). This suggests that even with 6-hour spin-up from 0000 UTC JMA reanalysis, the vortex is still too weak. The typhoon is significantly deeper in ExpGV (Figure 5(d)) and ExpVr (Figure 5(c)), with their MSLP being 934 and 950 hPa,

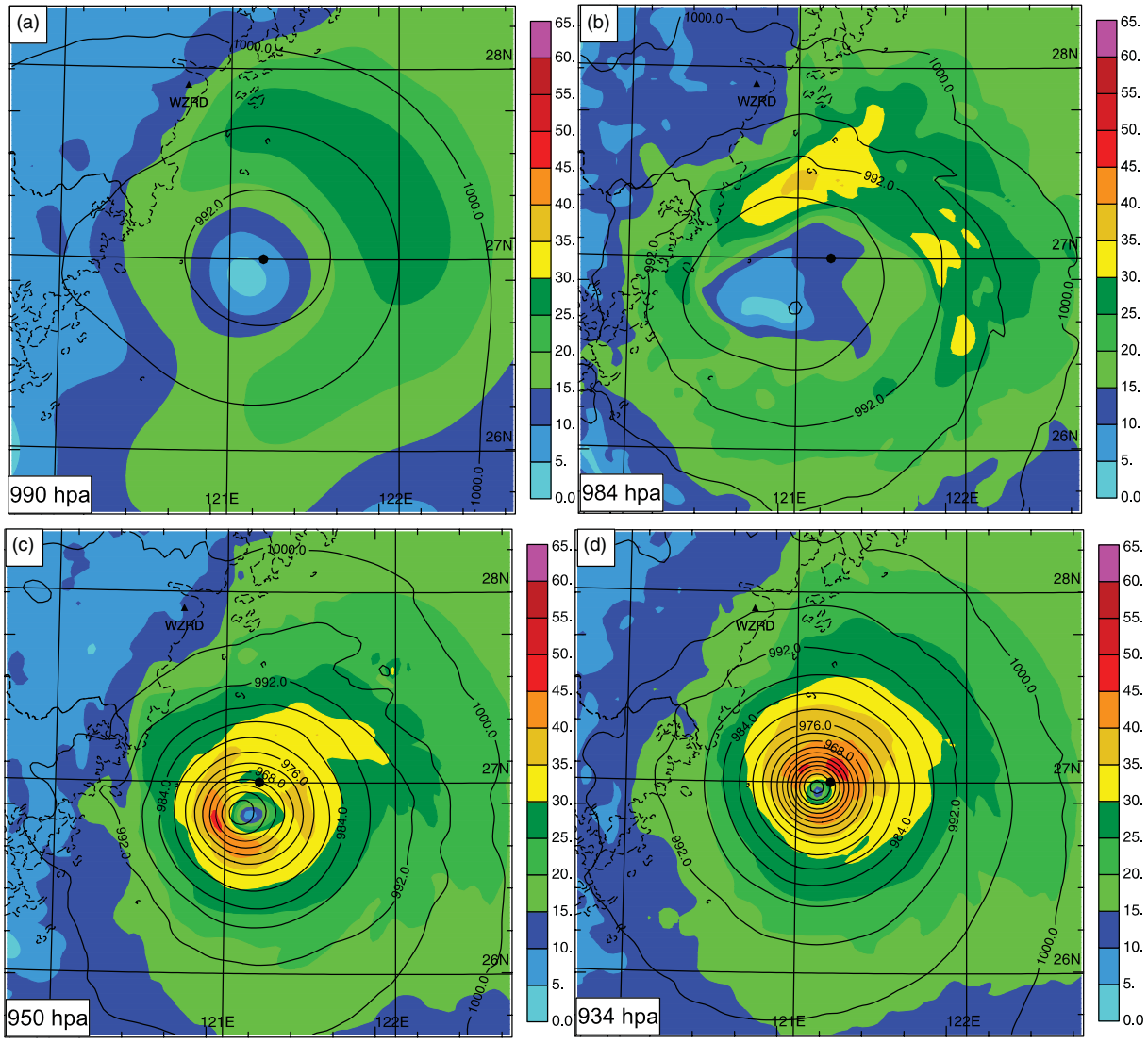

Figure 5. The sea-level pressure (SLP, thick solid contours) and surface wind speed (colour shaded contours, m s^{-1}) for super typhoon *Saomai* at 0600 UTC 10 August 2006, from experiments (a) CNTL, (b) CNTL00, (c) ExpVr, and (d) ExpGV. The black dot near the domain centre indicates the approximate centre location of the observed typhoon and the minimum pressure is given at the lower left corner of each panel.

respectively. The typhoon circulation in ExpGV is also the strongest, consistent with the lower MSLP. The horizontal wind speeds in both ExpGV and ExpVr exhibit wave number 1 asymmetry with similar MSW, but the locations of their peak winds are different. The high wind area in ExpGV is located in the northeast quadrant of the vortex, closer to the radar observations (not shown); in ExpVr, the high wind area is located in the southwest quadrant instead. Besides the improvement in intensity, the analysed typhoon centres are closer to the observed locations with radar data assimilation. The centre location improvement is most evident in ExpGV; the observed centre location is indicated by a black dot in Figure 5.

To examine the vertical structure of the analysed typhoon, east–west vertical cross-sections of horizontal wind speed through the typhoon centre are presented in Figure 6 for CNTL, ExpVr and ExpGV. In CNTL, the weak vortex circulation and the large eye are evident (Figure 6(a)). The vortex in ExpVr (Figure 6(b)) is much stronger, with a more upright eyewall than in CNTL. Assimilating V_{GBVTD} data in ExpGV (Figure 6(c)) results in an even more upright eyewall and the strong tangential winds extend to a much higher level than in ExpVr (Figure 6(b)).

To compare the axisymmetric structures, the azimuthal mean tangential winds and the horizontal temperature anomaly (defined at each level as the deviation from the temperature averaged over a horizontal area within a radius of 180 km, similar to Liu *et al.*, 1999) of the analysed typhoons are plotted in Figure 7; again the vortex circulation is much weaker and broader in CNTL (Figure 7(a)), while that in ExpGV is the strongest. Consistent with a stronger circulation, ExpGV also shows the strongest warm core in the eye region, with the maximum anomaly being at about 6 km, similar to those found in previous observations and simulations of intense TCs (Hawkins and Imbembo, 1976; Liu *et al.*, 1999; Halverson *et al.*, 2006). The vortex in ExpVr (Figure 7(b)) has a radius of maximum wind (RMW) of about 30 km, close to the best track value of about 20 km; a 49 m s^{-1} maximum tangential wind is found below 1.5 km, and a 12 K maximum temperature anomaly is at about 7 km. In ExpGV (Figure 7(c)), the vortex has a smaller RMW of about 20 km, a maximum mean wind speed of about 55 m s^{-1}, and a maximum temperature anomaly of

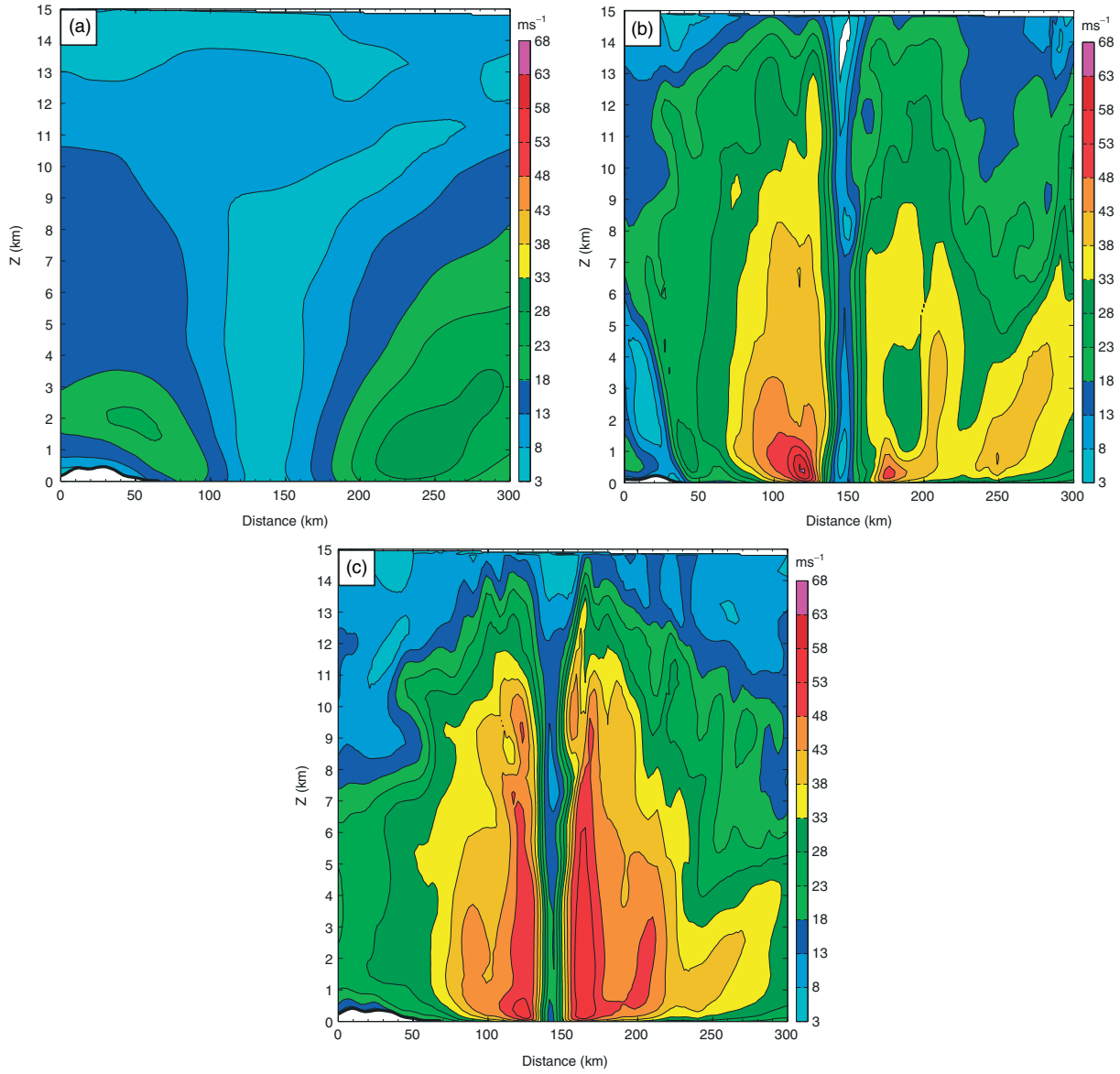

Figure 6. Horizontal wind speed (m s^{-1}) in the east–west vertical cross-sections through the analysed typhoon centres in Figure 5 for experiments (a) CNTL, (b) ExpVr, and (c) ExpGV.

about 20 K. It is also noted that a secondary wind maximum is found at a radius of about 55 km in ExpGV (Figure 7(c)), which is associated with the outer eyewall; such a secondary maximum is not found in ExpVr. Although the vertical structure cannot be directly verified by observations, the steepest slope of the RMW line associated with the smallest RMW in ExpGV is consistent with the study of Stern and Nolan (2009), where the slope of the RMW is found to be inversely proportional to the RMW. The more realistic vortex structure obtained in ExpGV can be attributed to a better representation of the vortex inner core circulation by the V_{GBVTD} wind data.

4. Forecast results

4.1. Impact of wind assimilation on typhoon structure forecast

We first examine the impact of assimilating V_{GBVTD} or V_{r} data on the predicted structure of *Saomai* (2006). Figure 8 shows the composite (column maximum) radar reflectivity and 3 km height wind fields at 3, 6, 9 and 12 hours of forecast from experiments CNTL, CNTL00, ExpVr and ExpGV, as compared to the corresponding reflectivity observations in the first row. At 0900 UTC – the 3-hour forecast time – the predicted vortex in CNTL (Figure 8(e)) and CNTL00 (Figure 8(i)) continues to be weaker and broader than that in assimilation experiments. The reflectivity is over-predicted in CNTL along a spurious rainband on the northwest side of the vortex (Figure 8(e)). We note that CNTL was able to quickly spin up precipitation within the first 1–2 hours of forecast, even though its initial condition from the JMA reanalyses did not contain any hydrometeor. In comparison, the 3-hour forecasts of the radar-assimilating experiments, ExpVr and ExpGV (Figure 8(m, q)), show tighter vortex circulations and rainbands located closer to the vortex centre.

By 1200 UTC – the 6-hour forecast time – *Saomai* had moved over land. The typhoon centre is now filled with precipitation after landfall, and the strong echo regions ($Z > 40$ dBZ) are now in the northeast and southeast quadrants of the typhoon (Figure 8(b)). *Saomai*'s centre

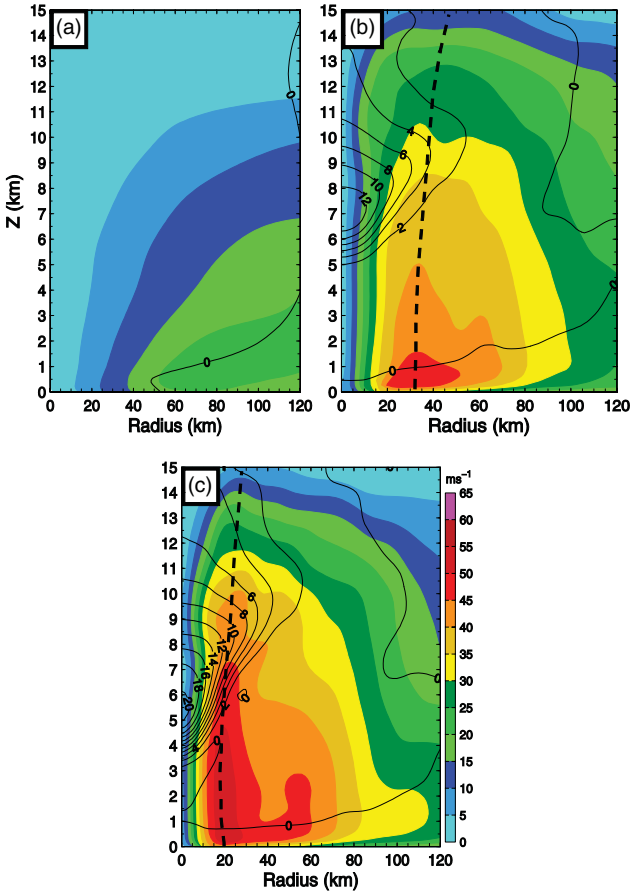

Figure 7. Azimuthally averaged tangential wind (shaded with the scale on the right) and temperature deviation from the horizontal mean (solid contours with intervals of 2 K) at 0600 UTC 10 August 2006 from experiments (a) CNTL, (b) ExpVr, and (c) ExpGV. Dashed lines in (b) and (c) indicate the axis of RMW.

in all three experiments had also made landfall by this time. The centre in ExpGV (Figure 8(r)) appears to be best positioned, while *Saomai*'s motion in CNTL and CNTL00 (ExpVr) appears faster (slower) than that in the best track data (Fig. 8(f, j, n)). The predicted reflectivity structure in CNTL continues to exhibit broad spiral rainband structures and the centre of the vortex has a large weak reflectivity hole. In CNTL00, the predicted reflectivity has a smaller areal coverage, mostly surrounding the precipitation-free vortex centre. In ExpVr, most of the strong reflectivity (>35 dBZ) is still offshore, inconsistent with radar observations, while in ExpGV the strong reflectivity is mostly over land and confined to a small region near the vortex centre, as observed.

At 9 hours of forecast, the precipitation pattern became more asymmetric (Figure 8(c)). The observed strong precipitation is now mostly located in the southeast half of the vortex, presumably due to the stronger moisture transport from the ocean on the southeast side, and some interaction with the terrain in Zhejiang Province (*Saomai* made landfall at the border of Zhejiang and Fujian Provinces, shown in Figure 1). On the west side of the vortex, there should be entrainment of drier air from the higher latitudes that tends to suppress precipitation.

The observed reflectivity structure is best captured by ExpGV. Both the reflectivity pattern and the position of strong reflectivity in the vortex agree very well with observations (Figure 8(s)). The reflectivity in CNTL remains rather broad and becomes disorganized (Figure 8(g)). The reflectivity patterns in ExpVr and CNTL00 look similar. They are closer to observations than CNTL but most of the high reflectivity is found in the eastern half of the vortex rather than on the southeast side. ExpVr also exhibits two rainbands within the high-reflectivity region which are not observed (Figure 8(o)). The vortex circulations in ExpGV and ExpVr still appear tighter than in CNTL and CNTL00.

At 12 hours of forecast, the precipitation is completely over land and the strong echo region remains concentrated in the southeast quadrant, as earlier. Again, the forecast of ExpGV has the best agreement with observations (Figure 8(t)), while that of CNTL has the worst agreement (Figure 8(h)). The vortex in CNTL is rather broad, while its precipitation region is significantly off-centred.

To better compare the structure and intensity among these experiments, the sea-level pressure and surface wind speed at 0900 UTC 10 August (3-hour forecast time) when the typhoon is near landfall are shown in Figure 9. It is clear that the forecast vortices in ExpGV and ExpVr are much more intense than that in CNTL or CNTL00, and the 948 hPa MSLP in ExpGV is closest to the best track MSLP of 935 hPa. CNTL (CNTL00) only predicted a 988 hPa (985 hPa) MSLP, with the strongest winds found at about 70 km from the centre. It is noted that the surface wind speeds from both radar-assimilating experiments exhibit a wave number 1 asymmetry, but their locations of peak winds are different. The high wind speeds in ExpGV are located in the northnortheast quadrant, while those in ExpVr are mostly in the eastern quadrant. In addition, the predicted typhoon centre in ExpGV is closer to the best track location (black dot) than those in other experiments.

South–north cross-sections of equivalent potential temperature (θ_e) and horizontal wind speed through the predicted typhoon centre at 3 hours of forecast are plotted in Figure 10 for CNTL, ExpVr and ExpGV. Consistent with results shown in Figure 9, the typhoon is weaker, with a very large eye in CNTL. Compared to CNTL (Figure 10(a)), the typhoon inner core in ExpVr (Figure 10(b)) and ExpGV (Figure 10(c)) is much better defined, with the narrow eye region extending vertically from surface to about 7–8 km height before expanding in diameter. High θ_e values are found in the eye region, indicating air of upper-level origin due to descent within the eye. High θ_e values are also found in the boundary layer. The low-level θ_e contours turn upward, with an outward slope that more or less follows the axis of maximum winds. Consistent with Figure 10, the azimuthal mean tangential wind and the horizontal temperature anomaly at this time also reveal an enhanced vortex in the forecasts of ExpVr (Figure 11(b)) and ExpGV (Figure 11(c)), accompanied by a clear warm core in the eye region. The maximum temperature anomaly is at about 7 km height. Wind speeds higher than 35 m s^{-1} extend to nearly 7 km height in ExpGV – higher than in ExpVr; the wind speed decreases rapidly above 7 km, consistent with the level of maximum temperature anomaly and the expected cyclostrophic balance. The maximum of warm core anomaly is about 16 K in ExpGV – higher than that in ExpVr. These features are consistent with the fact that ExpGV predicts a stronger typhoon than ExpVr. It is noted the maximum azimuthal mean wind below 1 km in ExpGV is slightly

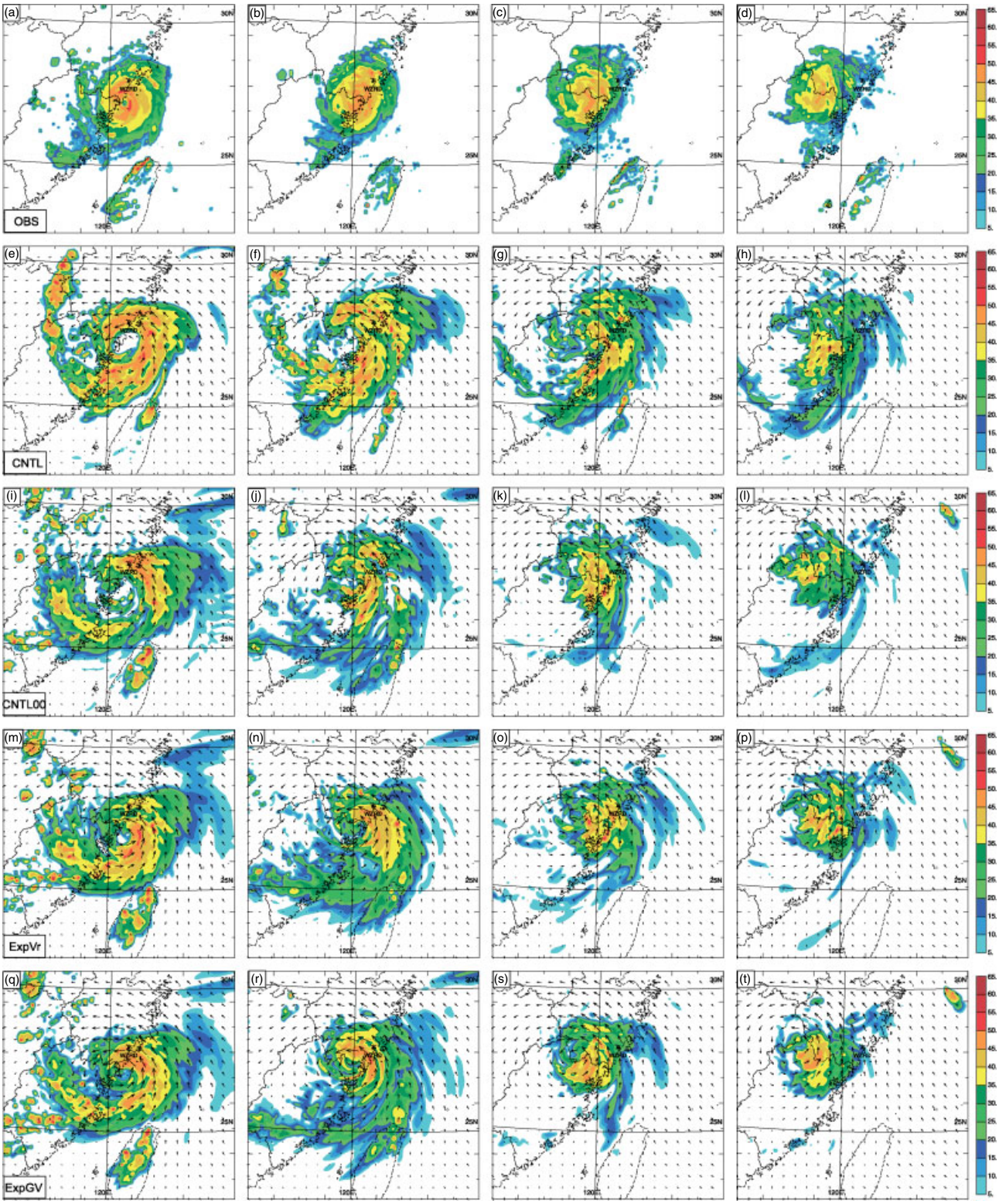

Figure 8. Observed (1st row) and predicted (other rows) composite (column maximum) reflectivity and the wind vectors at 3 km MSL corresponding to 3-hour (0900 UTC, 1st column), 6-hour (1200 UTC, 2nd column), 9-hour (1500 UTC, 3rd column) and 12-hour (1800 UTC, 4th column) forecasts, from experiments CNTL (2nd row), CNTL00 (3rd row), ExpVr (4th row), and ExpGV (5th row).

weaker than that in ExpVr, which can be attributed to the earlier landfall in ExpGV.

Overall, the radar-assimilating experiments have shown better predictions of the circulation and precipitation structures in *Saomai* up to the 12 h of forecast. The forecast assimilating V_{GBVTD} data is better than that assimilating V_{r} data.

4.2. *Track and intensity predictions*

The predicted typhoon track, MSW and MSLP from CNTL, CNTL00, ExpVr and ExpGV are plotted in Figure 12, together with the best track data for the 12-hour forecast period from 0600 UTC to 1800 UTC 10 August 2006. Figure 12(a) shows the predicted and observed tracks, while

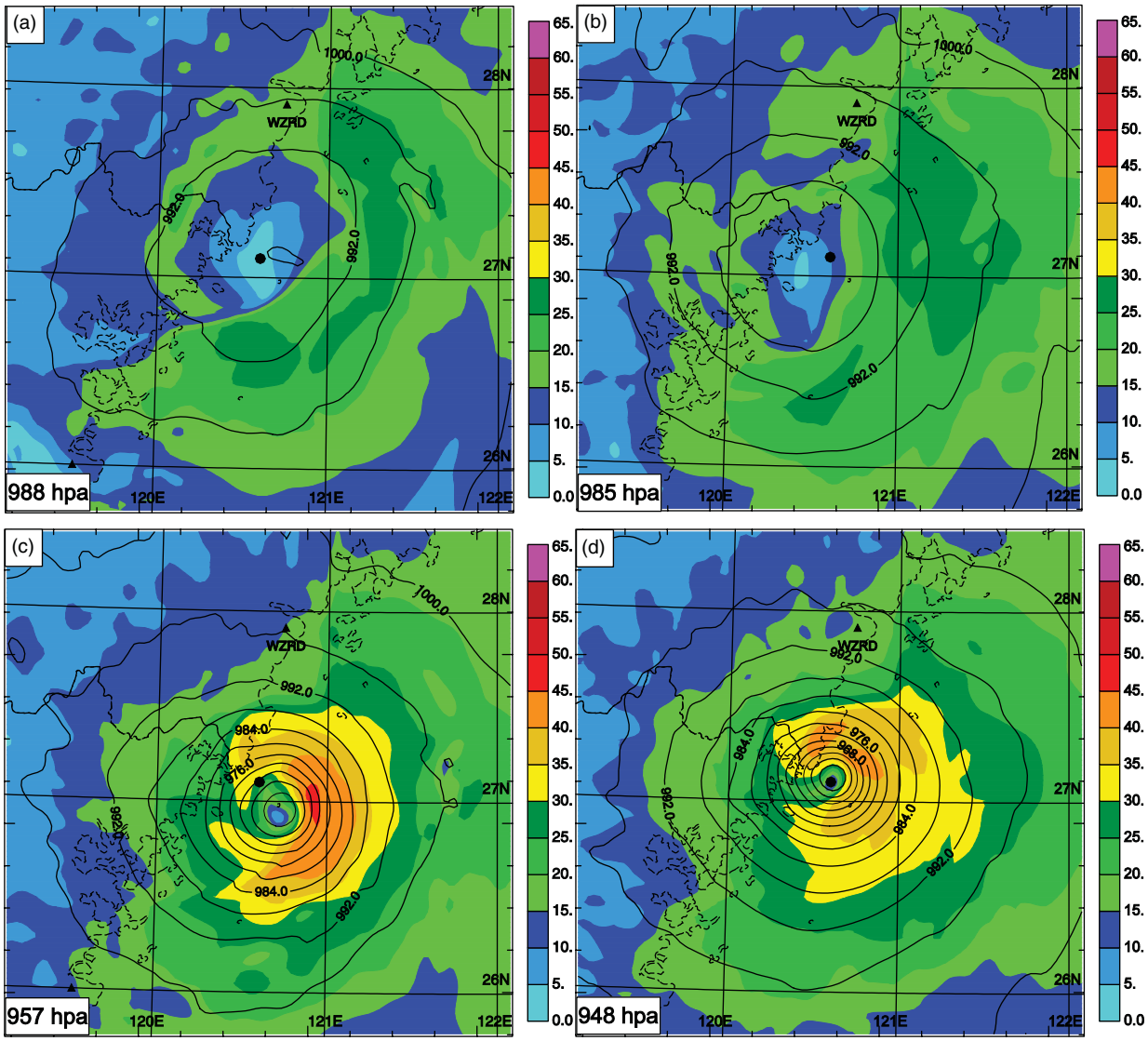

Figure 9. The 3-hour forecasts of SLP (thick solid contours), and surface wind speed (shaded contours, m s^{-1}) for super typhoon *Saomai* at 0900 UTC 10 August 2006, from experiments (a) CNTL, (b) CNTL00, (c) ExpVr, and (d) ExpGV. The black dot near the domain centre indicates the approximate centre location of observed typhoon and the minimum pressure is given in each panel.

Figure 12(b) shows the track errors (in km) at each forecast hour. In CNTL and CNTL00, the predicted typhoon tracks have a similarly northwestward bias (Figure 12(a)), resulting in a 12-hour mean error of about 36 km and 39 km (Figure 12(b)), respectively. In comparison, the 12-hour mean track error is reduced to 21 and 23 km in ExpVr and ExpGV (Figure 12(b)), respectively. In the first 4 hours of forecast, ExpGV shows the closest track to observations, presumably due to its best analysis of the initial storm structure and location, as indicated in Figure 5. After that time, the track error of ExpVr becomes the smallest among the three experiments. Such a switch in relative predicted track errors between ExpGV and ExpVr can be explained from their initial difference. As shown in Figure 5, there is a southward deviation of the vortex centre in the initial field of ExpVr, which happens to offset the northward deviation of the track during later forecasts, considering both ExpGV and ExpVr have a tendency to northward track forecast bias. Apparently, even though the radar data assimilated in this study cannot influence the large-scale environment, the assimilation of either V_{GBVTD} or V_{r} data does have a positive impact on the track forecasts, mainly through initializing a vortex with more realistic intensity and structure. Fovell *et al.* (2009) showed that the structure differences in simulated TCs can influence their motion within the same large-scale environment. The 'beta gyre' effect was quoted as the primary mechanism.

The best-track MSLP and MSW and those predicted by CNTL, CNTL00, ExpVr and ExpGV are plotted in Figure 12(c) and (d), respectively. Clearly, both CNTL and CNTL00 significantly under-predict the intensity in terms of both MSLP and MSW, mainly due to a weaker intensity in the initial condition. The radar-assimilating experiments show a notable improvement in intensity forecast. ExpGV shows an even better intensity forecast than ExpVr in terms of MSLP (Figure 12(c)) while the MSW is about the same in the final analyses and forecasts between the two experiments (Figure 12(d)). This again suggests that the assimilation of V_{GBVTD} data is more effective in improving the intensity of the overall vortex.

It is noted that the differences in MSLP among all assimilation experiments are largest at the initial time. By 8 hours, the difference between ExpGV and ExpVr becomes rather small (although their MSLPs are still significantly

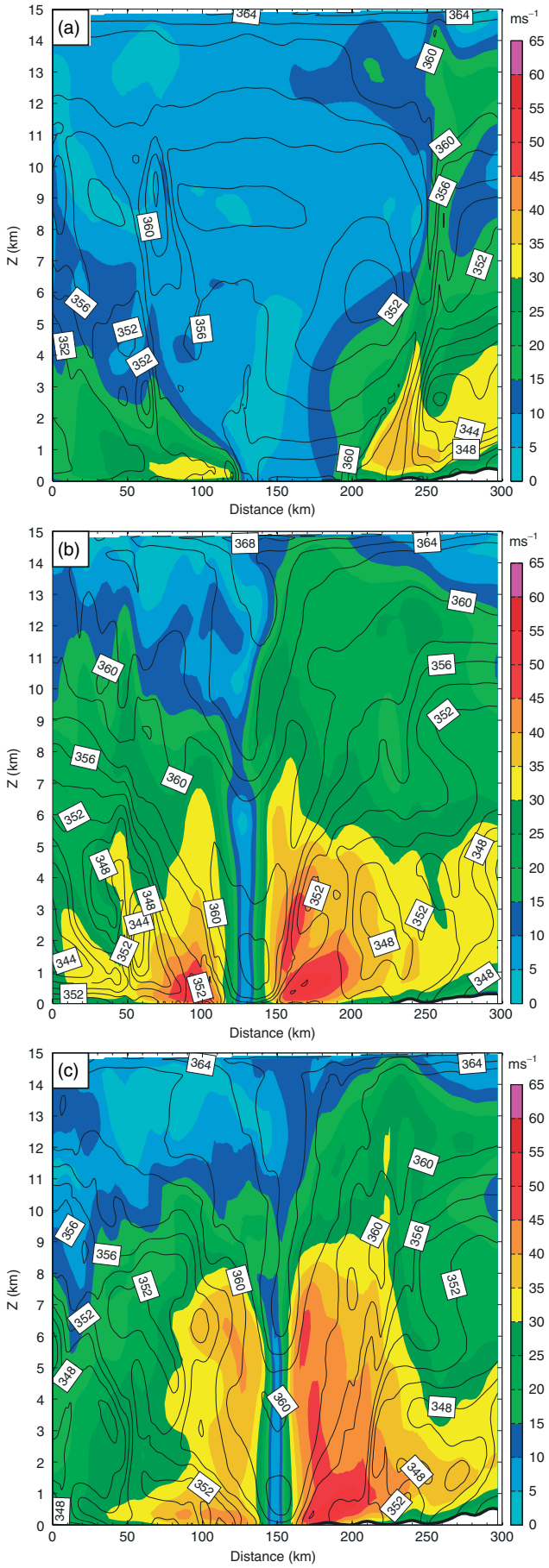

Figure 10. South–north vertical cross-sections of 3-hour forecast equivalent potential temperature (solid contours at 2 K intervals) and horizontal wind speed (shaded contours, m s^{-1}) valid at 0900 UTC 10 August 2006 from experiments (a) CNTL, (b) ExpVr, and (c) ExpGV.

lower than that of CNTL). This can be attributed to the rapid filling of typhoon *Saomai* after landfall. As low-pressure anomaly decreases in all experiments, the MSLP differences also decrease. A similar trend was found in the landfalling Hurricane Ike (Zhao and Xue, 2009). The intensity in terms of MSW shows a similar weakening trend, but the MSW in ExpVr decreases more slowly, particularly between 4 and 7 hours (Figure 12(d)). This can be attributed to the time lag in storm landfall in ExpVr compared to other experiments, which somewhat delays the vortex filling.

4.3. *Precipitation forecasting*

Inland flooding is the biggest hazard of landfalling TCs. Accurate precipitation forecast is therefore very important. Figure 13 compares the total accumulated precipitation during the 12-hour forecast period from the four experiments against high-resolution Automatic Weather Station rainfall observations (Figure 13(a)). It is clear that both CNTL (Figure 13(b)) and CNTL00 (Figure 13(c)) significantly underestimate the accumulated precipitation over land (where rainfall observations are available), along the path of the inner-core region. The observed precipitation shows a maximum near 27.5°N, close to WZRD radar (indicated by the black arrow in Figure 13(a)), and a band of strong precipitation along the border of Zhejiang and Fujian Provinces (cf. Figure 1). Compared with CNTL and CNTL00, the two radar-assimilating experiments show clear improvements in 12-hour precipitation forecast. The strong rainband north of the provincial border with a maximum reflectivity near WZRD is well captured, although the precipitation maximum south of the border is still underestimated in both experiments. Assimilating V_{GBVTD} data in ExpGV enhances the precipitation left of the storm track in northern Fujian (Figure 13(e)) more than that in ExpVr (Figure 13(d)). For lighter precipitation, the general pattern is similar to the available observations in all experiments.

For quantitative evaluation, equitable threat scores (ETS, also called Gilbert skill score; Schaefer, 1990) and biases of the 12-hour accumulated precipitation forecasts are plotted in Figure 14 as a function of precipitation thresholds for all four experiments. It is immediately clear that the radar-assimilating experiments obtain higher ETS scores than CNTL and CNTL00. Among them, ExpGV has the highest ETS scores for almost all thresholds; it also has the least precipitation bias, with the bias being close to one for thresholds between 0 and 200 mm. The two control experiments without radar data assimilation over-predict the weak precipitation and under-predict heavy precipitation, consistent with a weaker predicted typhoon. Their ETS scores drop quickly above the 50 mm threshold. CNTL00 shows somewhat higher ETSs than CNTL. ExpVr under-predicts the precipitation for all except the smallest thresholds (<20 mm). These quantitative scores again indicate that assimilating V_{GBVTD} data is most effective, while assimilating V_{r} data directly is also helpful, though to a lesser extent.

In addition to ETS scores for the accumulated precipitation, we also calculated the ETS scores for instantaneous composite (column maximum) radar reflectivity at 20 dBZ and 40 dBZ thresholds and for different forecast ranges (Figure 15). The composite reflectivity fields were constructed from level II data from multiple radars, some of which

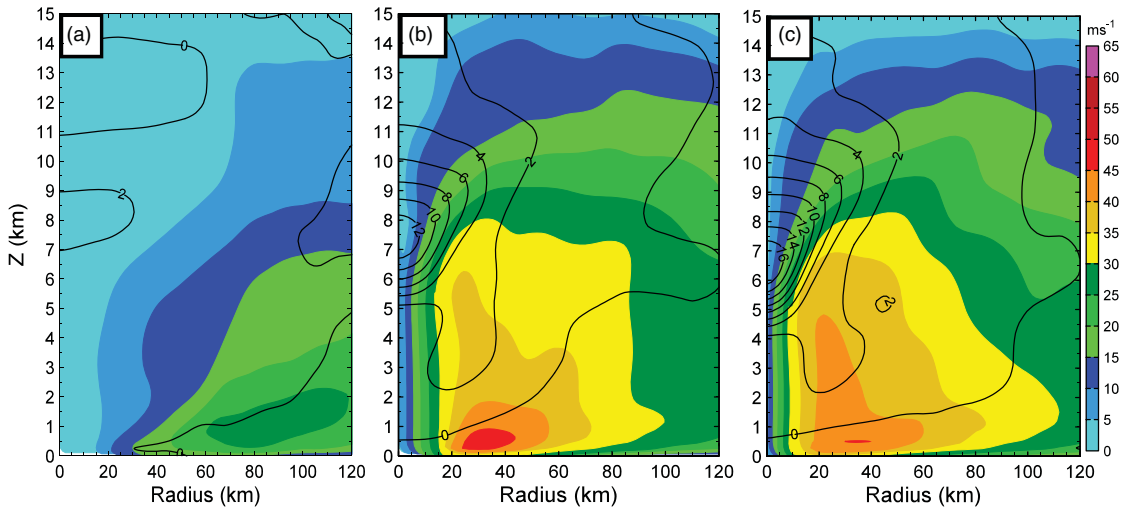

Figure 11. As in Figure 7, except at 0900 UTC 10 August 2006.

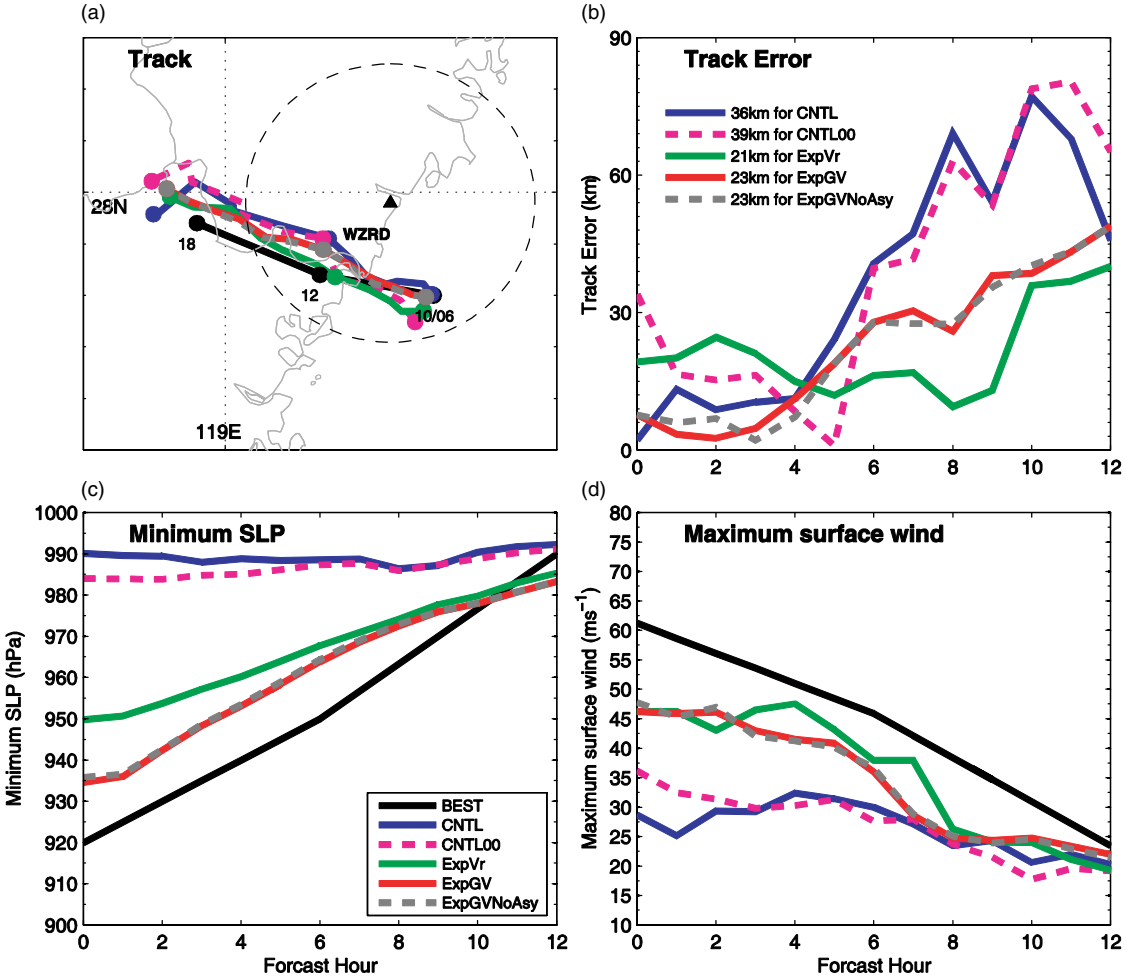

Figure 12. The 12-hour predicted (a) tracks, (b) track errors, (c) minimum SLP (hPa), and (d) maximum surface wind speed (m s^{-1}) of super typhoon *Saomai* from 0600 UTC to 1800 UTC August 10 2006. The large dashed circle in (a) is the 150 km range ring for WZRD. The numbers in (b) represent the mean track errors over the 12-hour forecast period. The labels in (a) and (d) are same as in (c).

were shown earlier in Figure 8. For the 20 dBZ threshold (Figure 15(a)), CNTL has slightly higher scores at hours 2 and 3 among all experiments, but its scores become the lowest afterwards. In comparison, CNTL00 has the lowest scores up to 5 hours; its scores are between those of ExpVr and ExpGV afterwards. ExpGV and ExpVr have similar scores before hour 4. The scores of ExpGV then steadily increase and remain significantly above those of CNTL and ExpVr afterwards. Its scores are about 0.5 between 7 and 12 hours, which are rather high values for high-resolution instantaneous reflectivity fields. For the 40 dBZ threshold (Figure 15(b)), CNTL has the lowest scores for almost all times, while the scores of ExpGV are consistently the highest. The score of CNTL00 is lower than ExpVr up to 5 hours, but

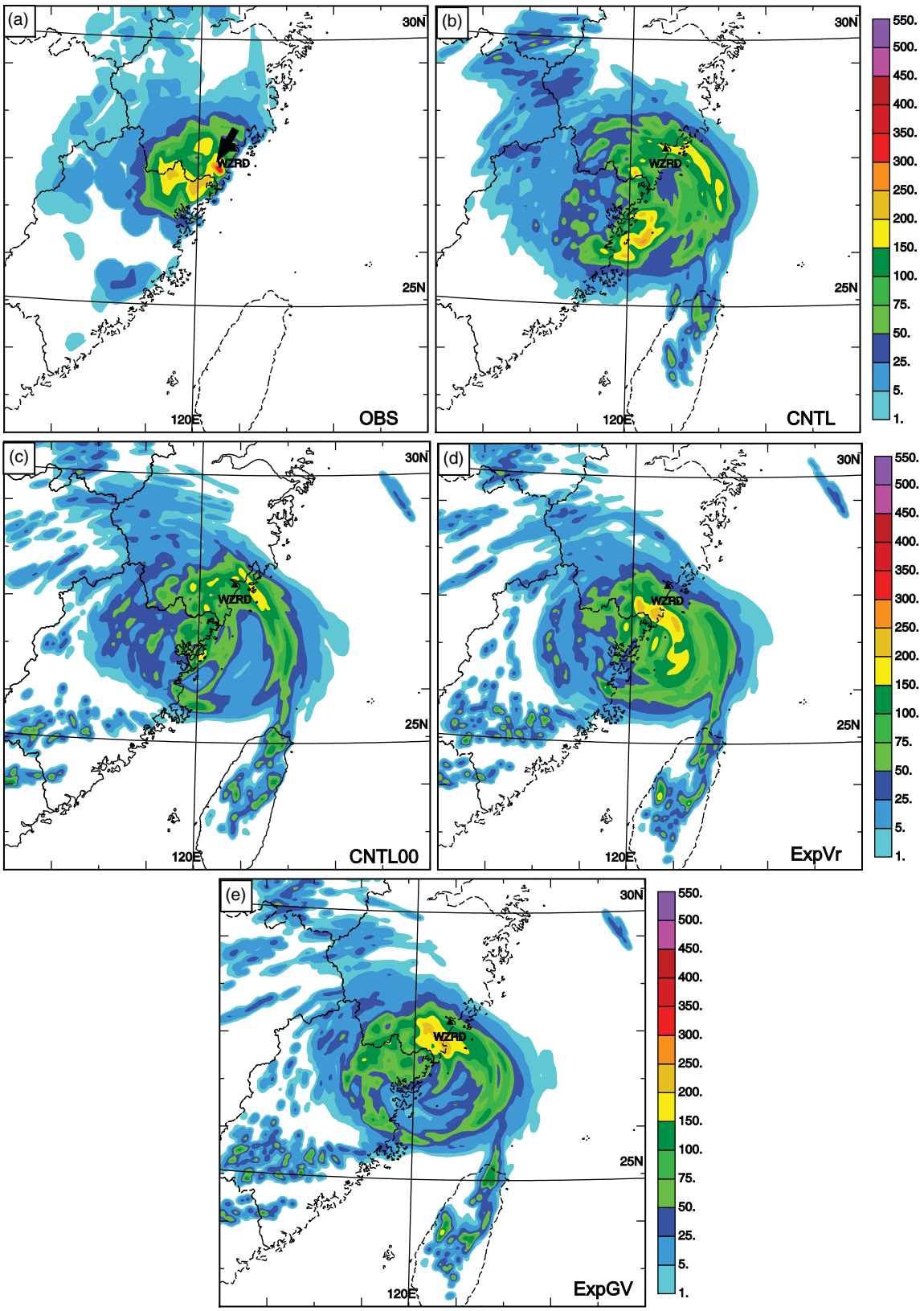

Figure 13. 12-hour accumulated precipitation (mm) valid at 1800 UTC 10 August 2006 from (a) automatic weather station hourly observations, and experiments (b) CNTL, (c) CNTL00, (d) ExpVr, and (e) ExpGV.

then exceeds its score until 10 hours. The scores of ExpVr are roughly halfway between those of ExpGV and CNTL. These scores indicate that the assimilation of radar data does improve precipitation forecast, with the assimilation of GBVTD data being more effective. These quantitative results are in agreement with our earlier subjective assessment.

4.4. *Role of the asymmetric component of GBVTD retrieval*

Past studies have shown the importance of asymmetry on tropical cyclone propagation and evolution (e.g. Wu and Wang, 2000, 2001). To evaluate the relative importance of the GBVTD-derived axisymmetric *versus* asymmetric

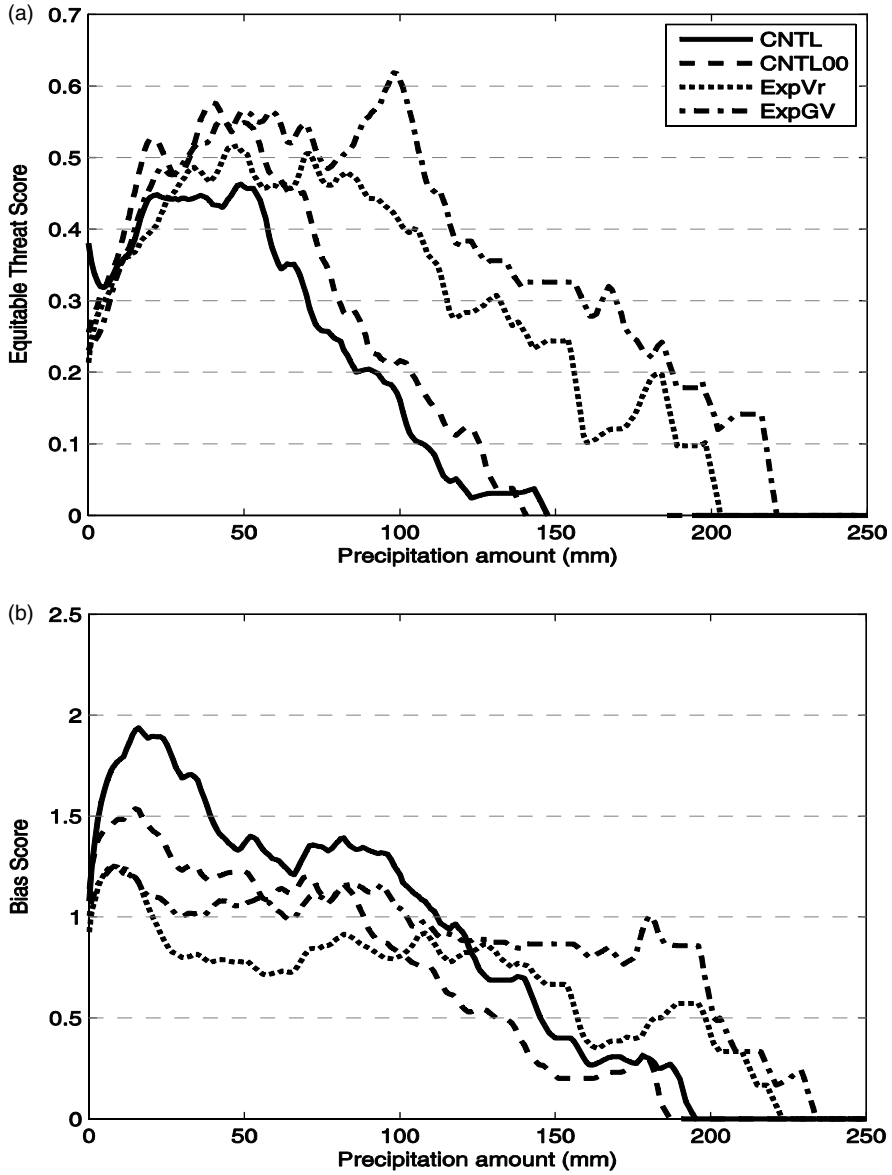

Figure 14. (a) Equitable threat scores and (b) biases of the 12-hour accumulated precipitation forecasts from CNTL, CNTL00, ExpVr, and ExpGV (shown in Figure 13) verified against automatic weather station hourly observations (as shown in Figure 13(a)) at 1800 UTC 10 August 2006.

wind components in data assimilation, we perform one additional experiment in which the asymmetric components are excluded from the retrieval. Basically, we want to assess how important are the structures above wave number 0 in the retrieval. We call this experiment ExpGVNoAsy. For brevity, we mainly present predicted track and intensity of this experiment in Figure 12. As shown, the predicted track and intensity in ExpGVNoAsy remain very close to those in ExpGV, suggesting that the axisymmetric wind component has a dominant role in improving the track and intensity forecasting in this case. We do note here that this conclusion may be case dependent, and more cases are needed to draw more definite or statistical conclusions.

5. Summary and conclusions

This study explores, for the first time, the assimilation of GBVTD-retrieved winds into a numerical weather prediction model. Experiments were performed at a 3 km horizontal resolution for the analysis and forecasting of super typhoon *Saomai* (2006), the strongest landfalling typhoon ever recorded in the offshore region of mainland China. The GBVTD-retrieved winds from the radial velocity data or the radial velocity data from single coastal operational weather radar at Wenzhou, Zhejiang Province, China, were assimilated over a 2-hour period prior to landfall; the ARPS 3DVAR/cloud analysis system was used with 30-minute assimilation cycles. Twelve-hour-long predictions were made from the final analyses. The results suggest the following.

The assimilation of GBVTD-retrieved winds (V_{GBVTD}) in experiment ExpGV results in much improved structure and intensity analyses over the control forecasts initialized directly from the JMA (Japan Meteorological Agency) mesoscale reanalysis, as well as over experiment ExpVr, which assimilates radial velocity (V_{r}) data directly. The ability of the GBVTD-based method in determining the full circle of vortex circulation in the inner-core region is the primary reason for ExpGV to outperform ExpVr with direct V_{r} assimilation. The GBVTD-retrieved winds have the advantages of not only providing the cross-beam

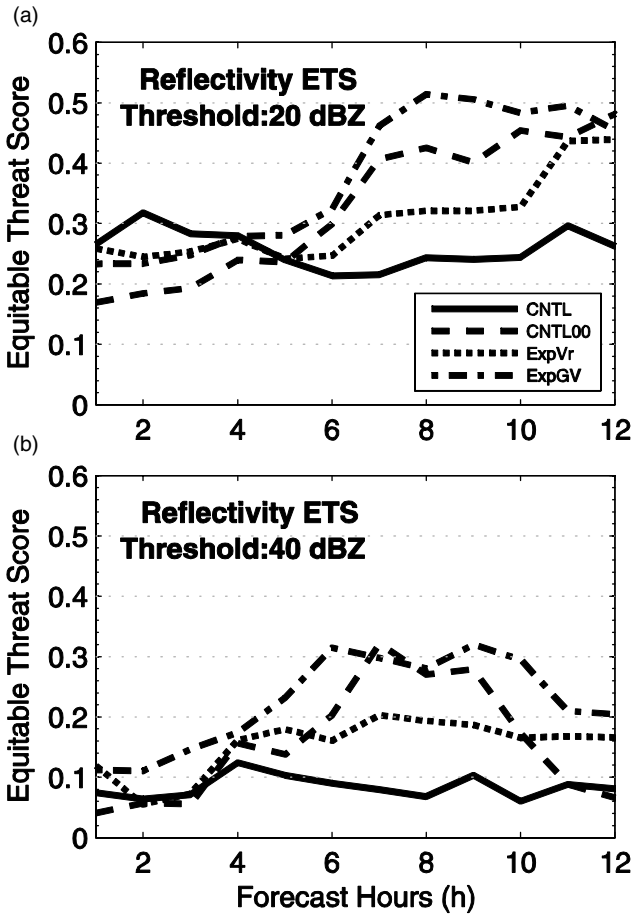

Figure 15. Equitable threat scores of predicted reflectivity for (a) 20 dBZ and (b) 40 dB*Z* threshold from experiments CNTL, CNTL00, ExpVr, and ExpGV, respectively.

wind component but also filling in data void regions when precipitation is unevenly distributed in the inner-core region. With the improvement in the initial conditions, the subsequent forecasts of typhoon intensity, track and precipitation are also improved. The improvements to both track and intensity predictions persist over the 12-hour forecast period, which is mostly after landfall. The subjective evaluations of the precipitation and circulation patterns and quantitative evaluations of precipitation and reflectivity against observations also support these findings. A further sensitivity experiment shows that the axisymmetric wind component in the GBVTD retrieval has a dominant impact on the prediction.

Although our conclusions here are based on a single landfalling typhoon case, the impact of V_{GBVTD} data on the structure, intensity, track and precipitation forecast of a landfalling typhoon is promising as long as enough radar data coverage is available for successful wind retrieval from the GBVTD algorithm. In fact, we have obtained preliminary results applying this method to Hurricane Ike (2008) studied by Zhao and Xue (2009) and the results are consistent with the findings here. Furthermore, our algorithm should be applicable to airborne radar data too, and therefore has the potential to improve tropical cyclone forecasts long before landfall. Work along this line is underway. Finally, we point out again that the GBVTD retrieval can be considered a much more sophisticated procedure for building a 'bogus' vortex. It directly uses radar wind observations, and tries to build a three-dimensional vortex that contains asymmetric circulations up to wave number 3 that best fit the radar observations, while traditional bogus vortex usually employs much simpler vortex models. As the GBVTD retrieval including quality control is computationally very fast, it can be completed within 1 minute using a current-generation single processor in a Linux computer, and it can be used in real time without much increase in the analysis cost. We also note that the GBVTD retrieval can be assimilated into the numerical model using more sophisticated data assimilation methods, such as 4DVAR (e.g. Zou and Xiao, 2000) and ensemble Kalman filter. In the latter case, dynamically more consistent pressure and temperature fields are expected; in our current case using 3DVAR for the wind analysis, we rely on frequent assimilation cycles to spin up other fields. In the future, we plan to compare our GBVTD procedure against bogus vortex methods, and test the algorithms using more cases to more robust conclusions.

Acknowledgements

This work was supported by NSF grants AGS-0802888, OCI-0905040, and funding from OU VPR Office, Office of Naval Researching grant N00014-10-1-013, N00014-10-1-0775, the National Natural Science Foundation of China (grants 40975011 and 40505004), the Social Commonwealth Research Program (GYHY201006007), the National Fundamental Research 973 Program (2009CB421502) and National Thousand People Plan of China. We appreciate the comments and suggestions provided by two anonymous reviewers that significantly improved the content and clarity of this manuscript. We would also like to acknowledge the China Meteorological Administration for collecting and archiving the radar data used in this study. K. Brewster provided assistance for the quality control of radar data. Y. Wang, J. Gao, G. Ge, N. Du, K. Zhu and Q. Wang are thanked for help with ARPS and ARPS3DVAR. Supercomputers at TACC, University of Texas, and at OSCER, University of Oklahoma, were used.

References

Brewster K. 2002. 'Recent advances in the diabatic initialization of a non-hydrostatic numerical model'. In *Preprints, 15th Conference on Numerical Weather Prediction/21st Conference on Severe Local Storms*, San Antonio, TX. American Meteorological Society, J6.3.

Brewster K, Hu M, Xue M, Gao J. 2005. 'Efficient assimilation of radar data at high resolution for short-range numerical weather prediction'. In *WWRP International Symposium on Nowcasting Very Short Range Forecasting*, Toulouse, CDROM 3.06.

Browning KA, Wexler R. 1968. A determination of kinematic properties of a wind field using Doppler radar. *J. Appl. Meteorol.* **7**: 105–113.

Davis C, Wang W, Chen SS, Chen YS, Corbosiero K, DeMaria M, Dudhia J, Holland G, Klemp J, Michalakes J, Reeves H, Rotunno R, Snyder C, Xiao QN, 2008. Prediction of landfalling hurricanes with the Advanced Hurricane WRF model. *Mon. Weather Rev.* **136**: 1990–2005.

Dong J, Xue M. 2010. 'Ensemble Kalman filter assimilation of coastal WSR-88D radar data and forecasting for hurricane Ike (2008)'. In *29th Conference on Hurricanes and Tropical Meteorology*, Tucson, AZ. American Meteorological Society, Paper No. P2.138.

Doviak RJ, Ray PS, Stauch RG, Miller LJ. 1976. Error estimation in wind fields derived from dual-Doppler radar measurement. *J. Appl. Meteorol.* **8**: 249–253.

Elsberry RL. 2005. Achievement of USWRP hurricane landfall research goal. *Bull. Am. Meteorol. Soc.* **86**: 643–645.

Fovell RG, Corbosiero KL, Kuo H-C. 2009. Cloud microphysics impact on hurricane track as revealed in idealized experiments. *J. Atmos. Sci.* **66**: 1764–1778.

Gao J-D, Xue M, Brewster K, Droegemeier KK. 2004. A three-dimensional variational data analysis method with recursive filter for Doppler radars. *J. Atmos. Ocean. Technol.* **21**: 457–469.

Halverson JB, Simpson J, Heymsfield G, Pierce H, Hock T, Ritchie L, 2006. Warm core structure of Hurricane Erin diagnosed from high altitude dropsondes during CAMEX-4. *J. Atmos. Sci.* **63**: 309–324.
Harasti PR, McAdie CJ, Dodge PP, Lee W-C, Tuttle J, Murillo ST, Marks FD. 2004. Real-time implementation of single-Doppler radar analysis methods for tropical cyclones: algorithm improvements and use with WSR-88D display data. *Weather Forecast.* **19**: 219–239.
Hawkins HF, Imbembo SM. 1976. The structure of a small, intense hurricane: Inez 1966. *Mon. Weather Rev.* **104**: 418–442.
Houze RA Jr, Chen SS, Smull BF, Lee W-C, Bell MM, 2007. Hurricane intensity and eyewall replacement. *Science* **315**: 1235–1239.
Hu M, Xue M, Brewster K, 2006. 3DVAR and cloud analysis with WSR-88D level-II data for the prediction of Fort Worth tornadic thunderstorms. Part I: Cloud analysis and its impact. *Mon. Weather Rev.* **134**: 675–698.
Kurihara Y, Bender MA, Ross RJ. 1993. An initialization scheme of hurricane models by vortex specification. *Mon. Weather Rev.* **121**: 2030–2045.
Lee JL, Lee WC, MacDonald AE. 2006. Estimating vertical velocity and radial flow from Doppler radar observations of tropical cyclones. *Q. J. R. Meteorol. Soc.* **132**: 125–145.
Lee WC, Bell MM. 2007. Rapid intensification, eyewall contraction, and breakdown of Hurricane Charley (2004) near landfall. *Geophys. Res. Lett.* **34**: L02802, DOI: 10.1029/2006GL027889.
Lee W-C Marks FD Jr, Carbone RE. 1994. Velocity track display: a technique to extract real-time tropical cyclone circulation using a single airborne Doppler radar. *J. Atmos. Ocean. Technol.* **11**: 337–356.
Lee W-C, Jou BJ-D, Chang P-L, Deng S-M, 1999. Tropical cyclone kinematic structure retrieved from single-Doppler radar observations. Part I: Interpretation of Doppler velocity patterns and the GBVTD technique. *Mon. Weather Rev.* **127**: 2419–2439.
Lee W-C, Jou BJD, Marks FD Jr. 2000. Tropical cyclone kinematic structure retrieved from single-Doppler radar observations. Part III: Evolution and structures of Typhoon Alex (1987). *Mon. Weather Rev.* **128**: 3982–4001.
Li W, Xie Y, Deng S-M, Wang Q. 2010. Application of the multigrid method to the two-dimensional Doppler radar radial velocity data assimilation. *J. Atmos. Ocean. Technol.* **27**: 319–332.
Liu Y, Zhang D-L, Yau MK. 1999. A multiscale numerical study of Hurricane Andrew (1992). Part II: Kinematics and inner-core structures. *Mon. Weather Rev.* **127**: 2597–2616.
Onogi K. 1998. A data quality control method using forecasted horizontal gradient and tendency in a NWP system: dynamic QC. *J. Meteorol. Soc. Jpn* **76**: 497–516.
Oye R, Mueller C, Smith C, 1995. 'Software for radar data translation, visualization, editing, and interpolation'. In *Preprints,27th Conference on Radar Meteorology*, Vail, CO. American Meteorological Society; 359–361.
Samsury CE, Zipser EJ. 1995. Secondary wind maxima in hurricanes: airflow and relationship to rainbands. *Mon. Weather Rev.* **123**: 3502–3517.
Schaefer JT. 1990. The critical success index as an indicator of warning skill. *Weather Forecast.* **5**: 570–575.
Segami A, Kurihara K, Nakamura H, Ueno M, Takano I, Tatsumi Y. 1989. Operational mesoscale weather prediction with Japan spectral model. *J. Meteorol. Soc. Jpn* **67**: 907–923.
Song J-J, Wang Y, Wu L. 2010. Trend discrepancies among three best track data sets of western North Pacific tropical cyclones. *J. Geophys. Res.* **115**: D12128, DOI: 10.1029/2009JD013058.
Stern DP, Nolan DS. 2009. Reexamining the vertical structure of tangential winds in tropical cyclones: observations and theory. *J. Atmos. Sci.* **66**: 3579–3600.
Tsuyuki T, Fujita T, 2002. 'Outline of the operational numerical weather prediction at the Japanese Meteorological Agency'. JMA Report, Tokyo.
Wu L, Wang B. 2000. A potential vorticity tendency diagnostic approach for tropical cyclone motion. *Mon. Weather Rev.* **128**: 1899–1911.
Wu L, Wang B. 2001. Movement and vertical coupling of adiabatic baroclinic tropical cyclones. *J Atmos Sci* **58**: 1801–1814.
Xiao Q, Kuo Y-H, Sun J, Lee W-C, Barker DM, Lim E. 2007. An approach of radar reflectivity data assimilation and its assessment with the inland QPF of typhoon Rusa (2002) at landfall. *J. Appl. Meteor. Climatol.* **46**: 14–22.
Xiao Q, Chen L, Zhang X. 2009. Evaluations of BDA scheme using the Advanced Research WRF (ARW) model. *J. Appl. Meteorol. Climatol.* **48**: 680–689.
Xue M, Droegemeier KK, Wong V, Shapiro A, Brewster K, Carr F, Weber D, Liu Y, Wang D-H. 2001. The Advanced Regional Prediction System (ARPS): a multiscale nonhydrostatic atmospheric simulation and prediction tool. Part II: Model physics and applications. *Meteorol. Atmos. Phys.* **76**: 143–165.
Xue M, Wang D-H, Gao J-D, Brewster K, Droegemeier KK. 2003. The Advanced Regional Prediction System (ARPS), storm-scale numerical weather prediction and data assimilation. *Meteor. Atmos. Phys.* **82**: 139–170.
Yu H, Hu C, Jiang L. 2007. Comparison of three tropical cyclone intensity datasets. *Acta Meteorol. Sin.* **21**: 121–128.
Zhang F, Weng Y, Sippel JA, Meng Z, Bishop CH. 2009. Cloud-resolving hurricane initialization and prediction through assimilation of Doppler radar observations with an ensemble Kalman filter. *Mon. Weather Rev.* **137**: 2105–2125.
Zhao K, Xue M. 2009. Assimilation of coastal Doppler radar data with the ARPS 3DVAR and cloud analysis for the prediction of Hurricane Ike (2008). *Geophys. Res. Lett.* **36**: L12803, DOI: 10.1029/2009GL038658.
Zhao K, Lee WC, Jou BJD. 2008. Single Doppler radar observation of the concentric eyewall in Typhoon *Saomai*, 2006, near landfall. *Geophys. Res. Lett.* **35**: L07807, DOI: 10.1029/2007GL032773.
Zhao Q, Jin Y. 2008. High-resolution radar data assimilation for Hurricane Isabel (2003) at landfall. *Bull. Am. Meteorol. Soc.* **89**: 1355–1372.
Zhao Q, Cook J, Xu Q, Harasti PR. 2006. Using radar wind observations to improve mesoscale numerical weather prediction. *Weather Forecast* **21**: 502–522.
Zhao Q, Cook J, Xu Q, Harasti PR. 2008. Improving short-term storm predictions by assimilating both radar radial-wind and reflectivity observations. *Weather Forecast* **23**: 373–391.
Zou X, Xiao Q. 2000. Studies on the initialization and simulation of a mature hurricane using a variational bogus data assimilation scheme. *J. Atmos. Sci.* **57**: 836–860.

